Research Article Vol. 30, No. 5 / 28 Feb 2022 / Optics Express 7477
Optics EXPRESS

Application of AdamSPGD algorithm to sensor-less adaptive optics in coherent free-space optical communication system

HENG ZHANG,[1,2] LI XU,[1,2] YONGFEI GUO,[1] JINGTAI CAO,[1] WEI LIU,[3] AND LEQIANG YANG[1,*]

[1] Changchun Institute of Optics, Fine Mechanics and Physics, Chinese Academy of Sciences, Changchun, Jilin 130033, China
[2] University of Chinese Academy of Sciences, Beijing 100049, China
[3] College of Communication Engineering, Jilin University, 5372 Nanhu Road, Changchun, Jilin 130012, China
[*] yanglq23@126.com

Abstract: Sensor-less adaptive optics based on stochastic parallel gradient descent (SPGD) is effective for the compensation of atmospheric disturbances in coherent free-space optical communication systems. However, SPGD converges slowly and easily falls into local extremes. Combining adaptive moment estimation and SPGD, we propose the AdamSPGD algorithm for efficient wavefront correction. Theoretical analysis and numerical simulations demonstrate that AdamSPGD can significantly increase the convergence speed, robustness, and dynamic ability, thereby more efficiently suppress the negative effects of atmospheric turbulence on mixing efficiency, bit error rate, and outage probability. Experimental results show that AdamSPGD reduces ~50% of iterations. The improved performances make the proposed algorithm suitable for SLAO to improve the quality of optical communications.

1. Introduction

In modern communications, coherent free-space optical communication (CFSOC) has attracted considerable attention owing to its longer relay distance, higher sensitivity, and better receiver selectivity compared with conventional free-space optical communication (FSOC) [1–5]. However, its application is significantly limited by atmospheric turbulence, owing to the intensity scintillation and wavefront phase distortion caused at the receiver, thereby reducing the mixing efficiency (ME) and increasing the bit error rate (BER) of the CFSOC system [6–8]. Adaptive optics (AO) technology has been utilized to compensate for wavefront aberrations caused by atmospheric turbulence and significant results have been achieved in many applications [9–14]. The Shack–Hartmann wavefront sensor (SH–WFS) is the most widely used wavefront sensor in conventional AO systems, and it directly determines the performance of the AO system in CFSOC. However, owing to the inherent shortcomings of its working principle, its measurement accuracy is reduced under strong atmospheric turbulence or low optical power, thereby directly affecting the system performance [15–18]. Therefore, a sensor-less adaptive optics (SLAO) system based on optimization algorithms has been proposed that directly optimizes the performance indicators based on the received images and does not require wavefront reconstruction [19,20].

In the SLAO system, the multidimensional optimization algorithm has a significant impact on the system performance. Although many algorithms have been proposed, stochastic parallel gradient descent (SPGD) is still extensively used in SLAO owing to its simple model, low number of parameters, and convenient implementation [21–23]. However, the convergence speed of SPGD is low and it easily falls into local extremes that limits its practical applications, particularly in complex systems [24]. In recent years, several types of SPGD improvements have been proposed

#451350 https://doi.org/10.1364/OE.451350
Journal © 2022 Received 15 Dec 2021; revised 3 Feb 2022; accepted 5 Feb 2022; published 18 Feb 2022

Optics EXPRESS

to alleviate the aforementioned problems. Lachinova et al. proposed the decoupled SPGD (DSPGD) algorithm to improve the convergence efficiency for the compensation of atmospheric phase aberrations in a tiled fiber array system. However, DSPGD necessitates prior knowledge of the performance metrics that limits its applications [25]. Wu et al. proposed a multi-perturbation SPGD with a fast-decent mode and a modal-basis updating mode for the enhancement of its effectiveness. However, this method requires the splitting of the incoming beam into N sub-beams and the use of N wavefront correctors that increases the complexity of the optical system [26]. Hu et al. proposed the adaptive SPGD (ASPGD) by integrating the momentum and adaptive gain coefficient for the control of a fast steering mirror (FSM), and achieved efficient fiber coupling. This method avoids the convergence to local extremum points and accelerates the convergence speed of SPGD to some extent [27]. Wang et al. conducted extensive research on SPGD in a fiber laser beam combining system. Yang et al. incorporated pattern recognition in SPGD to access whether the algorithm falls into in a local extreme [28]. They also adopted the momentum method with SPGD (MSPGD) to speed up the correction process of incoherent beam combination that can not only accelerate the efficiency of the iteration, but also maintain the stability of the combination [29]. Song et al. modified SPGD with the momentum term (MomSPGD) derived from the Newtonian equation to improve the convergence speed and disturbance immunity of coherent beam combination [30]. Che et al. proposed the AdmSPGD with adaptive gain and momentum based on the variation of the performance metrics in their previous practice, and significantly increased the convergence speed, robustness, and effective bandwidth in a fiber laser beam combining system [31]. Among these methods, improvements to SPGD are basically achieved by adding momentum terms and/or setting variable gain coefficients, and promising results have been achieved. However, their specific implementations and application areas vary, most of these methods are proposed for specific optical problems and cannot be directly applied to CFSOC systems to achieve adequate ME. Therefore, the optimization analysis and application of SPGD combined with adaptive moment estimation is lacking in CFSOC systems, and its effectiveness requires further verification and implementation.

To solve these problems, this study first analyzes the ME, BER, and outage probability of the CFSOC system according to coherent communication theory and accordingly establishes the relationship between the system performance indicators and the optimization algorithm fitness in SLAO. Thereafter, based on the adaptive moment estimation (Adam) in deep learning [32], a hybrid algorithm called AdamSPGD is proposed that combines Adam with SPGD to improve the correction speed and the robustness of SLAO. Here, the large Zernike polynomial modes are used to accurately represent the wavefront aberrations, and the correction effect is analyzed based on theory, numerical simulation, and experiments to validate the atmospheric turbulence suppression capability of the proposed algorithm. The results demonstrate that AdamSPGD can not only accelerate the correction speed by ~50%, but also improve the robustness of parameters, which is of great significance to the efficient wavefront correction of SLAO in CFSOC systems.

This paper is organized as follows: Section 2 provides the models of the CFSOC and SLAO systems, and analyzes and describes the working principles. Section 3 introduces the basic principles of the SPGD algorithm and the Adam optimizer. Thereafter, a novel hybrid algorithm, AdamSPGD is proposed that utilizes its characteristics. In Section 4, the phase aberration model in the CFSOC system is established, and the related simulations and comparisons are performed to demonstrate the improvement performance of AdamSPGD. Experiments were also conducted to verify the feasibility of the proposed algorithm by evaluating the far-field beam images in the developed SLAO system. Finally, the conclusions are presented in Section 5.

Optics EXPRESS

2. System model and theoretical analysis

2.1. CFSOC system model with SLAO

The functional block diagram of a typical CFSOC system with an SLAO is illustrated in Fig. 1. The laser source emits a modulated laser beam as a carrier signal. Thereafter, the beam is transmitted to the receiving terminal through an atmospheric link. Its frequency is mixed with a local oscillation signal for the generation of an intermediate frequency signal. A demodulator and a digital signal processor are used to complete the subsequent processing. During laser transmission, the wavefront is distorted by atmospheric turbulence. To compensate for the influence of atmospheric turbulence, an SLAO system is introduced in the receiving terminal.

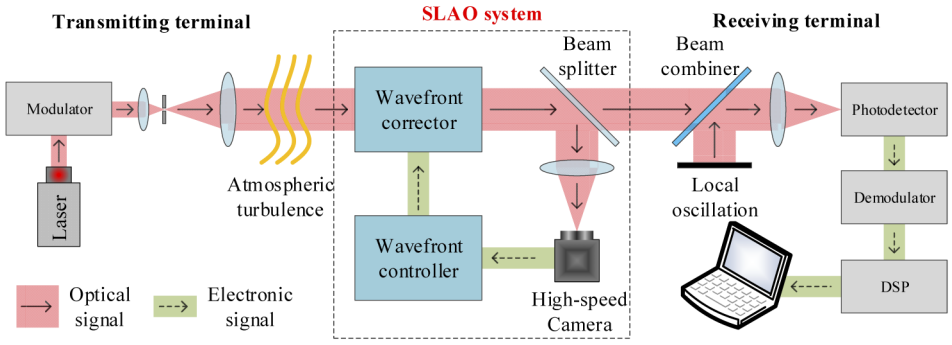

Fig. 1. Conventional CFSOC system with SLAO.

A schematic of the SLAO system is shown in Fig. 2. The beam steering unit (BSU) is mainly used to speedily capture and track the beam and correct the large skew of the beam, such as tilts and jitters, using the FSM. After the BSU, the laser carrier signal is concentrated in the deformable mirror (DM) and subsequently split into two beams by a beam splitter (BS). The energy concentration rate of the speckle images captured by a high-speed camera (HSC) reflects the current performance of the system. The high-order aberration correction computer (HCC) runs the selected optimization algorithm according to the images and generates a voltage control signal. The signal is amplified to a suitable voltage range using high-voltage amplifiers to control the DM for the correction of the distorted wavefront. After turbulence compensation by the SLAO system, the performance of the CFSOC can be improved based on a higher ME and lower BER. In this study, we consider only the high-order aberration correction unit [9,16].

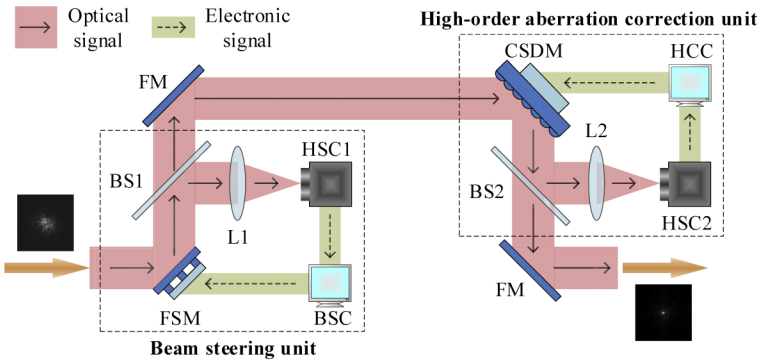

Fig. 2. Principle schematic of SLAO system.

Optics EXPRESS

2.2. DM model in SLAO

In this study, a 97-element continuous surface DM (CSDM) was designed and manufactured by us for use as the wavefront corrector. The working principle of the CSDM is essentially the change in the surface shape of the mirror in real time according to the control voltage for the correction of wavefront aberrations. Generally, the influence function of the CSDM is approximated by the Gaussian model:

$$S_j(x,y) = \exp\left\{\ln\omega\left[\frac{1}{d}\sqrt{(x-x_j)^2+(y-y_j)^2}\right]^{\alpha}\right\}, \tag{1}$$

where ω is the coupling coefficient of adjacent actuators, (x_j, y_j) is the center coordinate of the jth actuator, d is the normalized interval between the adjacent actuators, and α is the Gaussian index. The aberration generated by the CSDM with 97 actuators φ(x, y) is given by

$$\varphi(x,y) = \sum_{j=1}^{97} u_j S_j(x,y), \tag{2}$$

where u_j is the voltage of the jth actuator that is evenly distributed in the range of the maximum possible voltage and is linear with φ(x, y).

2.3. Theoretical basis of the CFSOC

In the CFSOC system, ME and BER are effective indicators for the evaluation of the system performance, and it is important to analyze these metrics to guide the determination of performance fitness in the SLAO algorithm.

Based on our previous work [9,14], the ME is approximated to the Strehl ratio (SR) of the far-field images defined by the ratio of the far-field encircled energy to the diffraction-limited encircled energy. The relationship between the ME and the average residual wavefront variance can be expressed as

$$ME \propto SR = \exp\left\{-\left[\alpha_F\left(\frac{d}{r_0}\right)^{5/3} + \kappa\left(\frac{f_G}{f_{3dB}}\right)^{5/3}\right]\right\}, \tag{3}$$

where α_F is the fitting error coefficient, r_0 denotes the atmospheric coherent length, d is the equivalent interval of the actuator interval projected on the entrance pupil of the receiving antenna, κ is a constant equal to 1 for a plane wave, f_{3dB} denotes the CLCB, and f_G represents the Greenwood frequency.

The BER of the synchronous binary phase shift keying (BPSK) coherent detection can be expressed as [5]

$$BER = \frac{1}{2}erfc\left(\sqrt{ME \cdot 2N_p\delta}\right), \tag{4}$$

where the function *erfc* represents the complementary error function, δ represents the quantum efficiency of the receiver detector, and N_p is the number of photons received within a signal bit.

Outage probability is another important performance criterion, defined as the probability that the instantaneous SNR is below a specified threshold that can be found in [7]:

$$P_{outage}(\gamma_T) = \Pr\{\gamma<\gamma_T\} = \int_0^{\gamma_T} f_\gamma(\gamma)d\gamma, \tag{5}$$

where $\Pr\{\cdot\}$ denotes the probability of an event, γ_T is a predefined outage probability threshold, and $f_\gamma(\gamma)$ is the PDF of the instantaneous SNR. The instantaneous combiner SNR is independent of the local oscillator power for a large local oscillator power, and the local oscillator power does not affect the CFSOC system performance [33]. Thus, γ is the SNR of the received optical signal.

Optics EXPRESS

3. AdamSPGD algorithm in SLAO

3.1. Fitness

For the use of optimization algorithms in SLAO, it is necessary to establish a connection between the optimization fitness and the system evaluation indicators of the CFSOC system. As the laser carrier signal is transmitted through the atmospheric channel, we assume that the initial wavefront aberrations are expressed as $\varphi_0(r,\theta)$, and the solutions of the algorithms are 97-dimension vectors $u = \{ u_1, u_2, \ldots, u_{97} \}$, where each component in the vector represents the control voltage of each actuator in the CSDM. Thereafter, we continuously update these solutions and generate the compensation phase $\varphi(r,\theta)$ according to Eq. (2) to compensate for the aberrations, and the residual phase aberrations can be given by $\phi(r,\theta) = \varphi_0(r,\theta) - \varphi(r,\theta)$. According to the analysis in Section2.3, this study considers the SR of $\phi(r,\theta)$ as the fitness J in algorithms to simplify the calculation [2]. The aim of the SLAO system is to optimize J to its ideal value. In the following sections, obtaining the maximum J through algorithms, we determine the optimum voltage signals u and the best ME of the CFSOC system.

3.2. AdamSPGD

The process of wavefront aberration compensation in SLAO based on conventional SPGD can be described in the following steps. First, the gradient estimation is realized by applying random low perturbation voltages $\Delta u^{(k)} = \{ \Delta u_1, \Delta u_2, \ldots, \Delta u_{97} \}$ that satisfy the Bernoulli distribution to the CSDM control voltage vectors $u^{(k-1)} = \{ u_1^{(k-1)}, u_2^{(k-1)}, \ldots, u_{97}^{(k-1)} \}$, simultaneously. The disturbances $\Delta u^{(k)}$ have a fixed amplitude, that is, $|\Delta u^{(k)}| = \Delta u$. Using the perturbed indicator values $J_{\pm}^{(k)} = J(u^{(k-1)} \pm \Delta u^{(k)})$, we can calculate the variation of the performance metric $\Delta J^{(k)} = J_{+}^{(k)} - J_{-}^{(k)}$. The iterative formula for updating the CSDM control voltages can be expressed as

$$u^{(k)} = u^{(k-1)} + \gamma \Delta u^{(k)} \Delta J^{(k)}, \tag{6}$$

where the superscript k denotes the number of iterations, and γ is the positive gain coefficient. $u^{(k)}$ updates along the direction of the gradient descent, and the performance metric J reaches an extremum after multiple iterations. The conventional SPGD only considers the current update vector, facilitating the formation of a local extremum and the gradual convergence.

The Adam proposed by Kingma is a method for the efficient stochastic optimization that combines the advantages of AdaGrad for addressing sparse gradients and RMSProp for managing non-stationary objectives [32]. Based on the adaptive moment estimation in Adam, we embed it into the SPGD and propose a novel AdamSPGD algorithm to accelerate convergence.

In AdamSPGD, first we approximate the gradient as [27]

$$g^{(k)} = \partial J^{(k)} / \partial u^{(k)} = \Delta J^{(k)} \cdot \Delta u^{(k)} / (\Delta u)^2. \tag{7}$$

Thereafter, we introduce the 1st momentum term (the mean) and the 2nd momentum term (the uncentered variance) of the gradient and update the exponential moving averages of the gradient $m^{(k)}$ and the squared gradient $v^{(k)}$ with hyper-parameters β_1 and β_2 to control the exponential decay rates. Thereafter, the initialization bias correction strategy is utilized to avoid moment estimates leading to zero during the initial iterations and to obtain the bias-corrected estimates $\hat{m}^{(k)}$ and $\hat{v}^{(k)}$. The relevant formulas are as follows:

$$m^{(k)} = \beta_1 m^{(k-1)} + (1 - \beta_1) g^{(k)}, \tag{8}$$

$$v^{(k)} = \beta_2 v^{(k-1)} + (1 - \beta_2)(g^{(k)})^2, \tag{9}$$

$$\widehat{m}^{(k)} = m^{(k)} / [1 - {\beta_1}^k], \tag{10}$$

$$\widehat{v}^{(k)} = v^{(k)} / [1 - {\beta_2}^k]. \tag{11}$$

The $\hat{m}^{(k)}$ depends on both the current gradient and the previous gradients, and enables averaging out the oscillation along the short axis. The $\hat{v}^{(k)}$ adds the weighted square results of the past

Optics EXPRESS

gradients that indicates the uncentered variance of the gradients. During the updating process, we divide the 2nd momentum term to adaptively search for a suitable gain rate. As discussed above, we update the CSDM control voltage vectors using AdamSPGD, as follows:

$$u^{(k)} = u^{(k-1)} + \alpha \widehat{m}^{(k)} / \left(\sqrt{\widehat{v}^{(k)}} + \varepsilon \right), \tag{12}$$

where α is the learning rate, and ε is a small constant usually set to 10^{-8} that is used to avoid numerical problems.

The implementation of the AdamSPGD algorithm for SLAO is comprehensively described in Algorithm 1.

Algorithm 1 Procedure of the AdamSPGD algorithm

Input: The learning rate α, the hyper-parameters β_1 and β_2, the constant ε, the amplitude of random perturbation voltages Δu, and the maximal number of iterations N.

Output: Calculated control voltage vectors of CSDM $u = \{u_1, u_2, ..., u_{97}\}$.

1: Initialize control voltage vectors $u^{(0)}$, the 1st momentum term $m^{(0)}$, the 2nd momentum term $v^{(0)}$

2: **for** $k = 1, ..., N$ **do**

3: Randomly generate the perturbed voltages obeying the Bernoulli distribution $\Delta u^{(k)}$

4: Obtain the evaluation functions under perturbation voltage $J_{\pm}^{(k)} = J\left(u^{(k-1)} \pm \Delta u^{(k)}\right)$

5: Obtain the change in the evaluation function $\Delta J^{(k)} = J_{+}^{(k)} - J_{-}^{(k)}$

6: Calculate the gradient $g^{(k)}$ (see Eq. (7))

7: Calculate the bias-corrected 1st momentum term $\widehat{m}^{(k)}$ (Eq. (8) and Eq. (10))

8: Calculate the bias-corrected 2st momentum term $\widehat{v}^{(k)}$ (Eq. (9) and Eq. (11))

9: Update the control voltage $u^{(k)}$ (see Eq. (12))

10: **end for**

Theoretically, the AdamSPGD algorithm improves the gain factor and gradient estimation compared with the SPGD algorithm. The update direction can be adjusted by the momentum factor that facilitates acceleration in the relevant direction and dampening of oscillations. The gain coefficients are adjusted adaptively during iterations in real time that enhances the convergence speed of corrections. The following simulations focus on the correction speed and robustness of the two algorithms.

4. Simulation and experiment

4.1. Simulation analysis

Zernike polynomials are generally adopted to decompose the distorted wavefront phase into the sum of weighted orthogonal polynomials that represent various types of aberrations. The wavefront phase φ_0(r,θ) can be expressed as follows [34]:

$$\varphi_0(r, \theta) = a_0 + \sum_{i=1}^{\infty} a_i Z_i(r, \theta). \tag{13}$$

In Zernike polynomials, the 0th term and $Z_1(r, \theta)$, $Z_2(r, \theta)$ represent the piston and tilt aberrations along the X and Y directions, respectively, that can be directly corrected by BSU. Because the higher Zernike polynomial modes may have better fitting accuracy, the 3th to 35th terms in Zernike polynomials are modeled as the distorted wavefront in our simulations, to simulate atmospheric turbulence. The voltages of the 97-element CSDM are algorithmically calculated to compensate for wavefront aberrations.

Optics EXPRESS

In the simulations, the default λ was set to 635 nm and D/r0 = 10. According to Roddier's method [35], we randomly generate initial Zernike coefficients from $a_3 - a_{35}$, as shown in **Fig. 3(a)**. The corresponding phase planes of the original wavefront and the original point spread function (PSF) are shown in **Fig. 3(b)** and **Fig. 3(c)**, respectively. The ME of this wavefront aberration is 0.2038 that will be used to compare the performance of the algorithms in the subsequent simulations. To facilitate our observation, the simulation results treat the optimization objective as the ME.

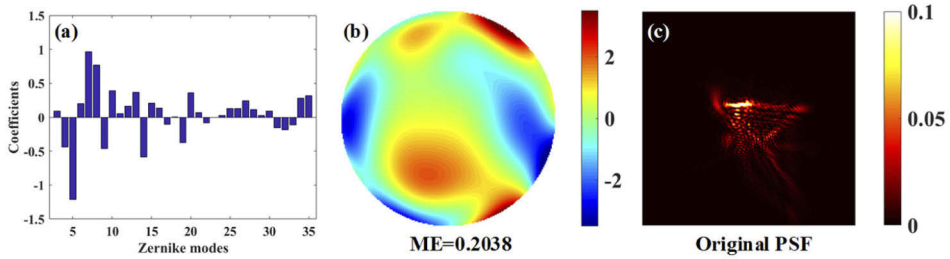

Fig. 3. Random set of simulated data. (a) Initial Zernike coefficients of the wavefront aberration. (b) Corresponding phase plane of the original wavefront. (c) Original PSF.

The corresponding residual wavefront aberrations and PSFs after correction under different iterations using AdamSPGD are shown in **Fig. 4**. The ME value obtained increases from 0.2038 to 0.8980 after 200 iterations that is 4.4 times that before compensation. Clearly, most of the distortion is compensated adequately by the AdamSPGD.

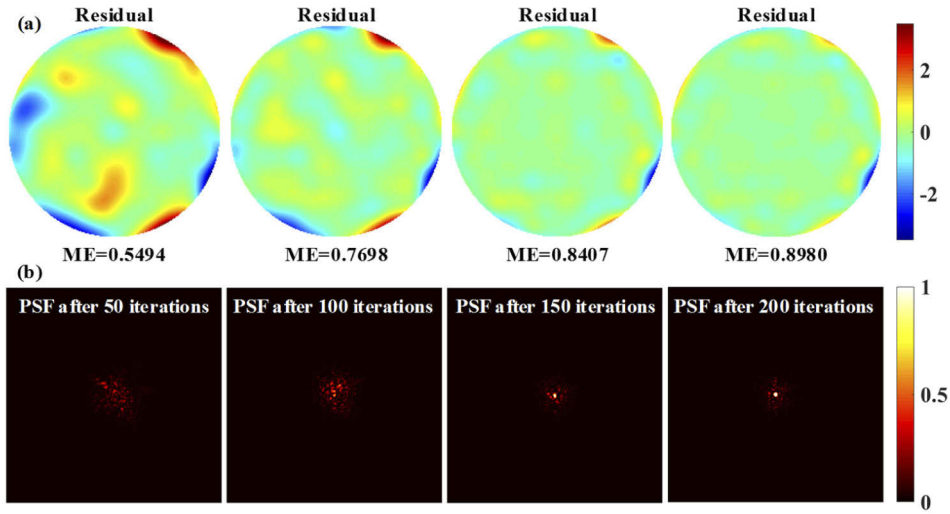

Fig. 4. Wavefront correction results under different iterations. (a) Phase plane of the residual wavefront aberrations after 50, 100, 150, and 200 iterations (left to right). (b) Corresponding PSFs in (a).

In the following simulations, the normalized ME based on 0.8 is used as the index, rather than the absolute value of ME, for the observation of the features of the algorithms more intuitively [36]. Considering the randomness of the method, we executed each simulation 100 times.

The optimization curves of the SPGD and AdamSPGD under their optimal parameters are shown in **Fig. 5**. Positive gain coefficient $\gamma = 2$, learning rate $\alpha = 0.1$, hyper-parameter

Optics EXPRESS

$\beta_1 = 0.999$ and $\beta_2 = 0.9$ as suggested in Ref. [32], constant $\varepsilon = 10^{-8}$, and the amplitude of random perturbation voltages $\Delta u = 0.5$.

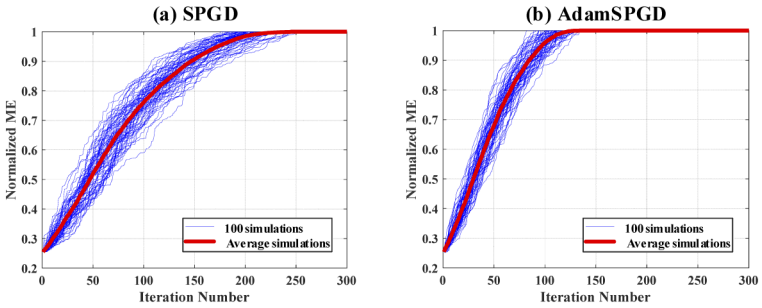

Fig. 5. Comparison of wavefront correction results: (a) SPGD (b) AdamSPGD.

As shown in **Fig. 5**, both algorithms can effectively compensate for aberrations. The SPGD converges after a minimum of 177 iterations, and a maximum of 252 iterations in the worst case, averaging at 208 iterations. AdamSPGD converges after a minimum of 82 iterations and a maximum of 136 iterations, with an average of 112 iterations that is 53.85% of the that in case of SPGD. In addition, the results of the SPGD fluctuate significantly because they significantly depend on the random disturbance at each iteration and the current gradient. AdamSPGD considers both the current gradient and historical gradients in the iteration process, thereby reducing the impact of randomness. Overall, AdamSPGD converges faster than SPGD, and is more robust to the randomness of the disturbance.

Assuming that the quantum efficiency δ is equal to 1 and the N_p is 12, the BER can be calculated according to Eq. (4). The variation curves of the system BER based on SPGD and AdamSPGD with the number of iterations are illustrated in **Fig. 6**.

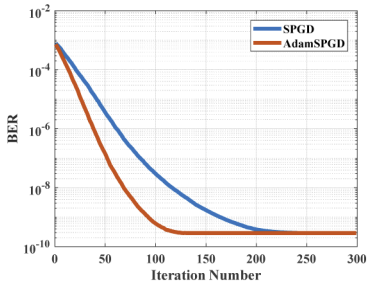

Fig. 6. Comparison of system BER between SPGD and AdamSPGD.

From **Fig. 6**, it is noted that the BER performance is substantially improved after the SLAO system compensates for the wavefront phase distortion. The values of BER dropped from approximately 10^{-2} to 10^{-9} after 92 iterations in case of AdamSPGD. Owing to the limitation of SPGD, the BER value cannot be suppressed below 10^{-9} in 164 iterations.

We also analyze the change in the outage probability with the number of iterations according to Eq. (5) when using the two algorithms; γ_T was set to 10 dB. The outage probability curves are shown in **Fig. 7**.

As shown in **Fig. 7**, the outage probability can be drastically suppressed to $\sim 10^{-3}$ after the SLAO corrections based on the two algorithms. Evidently, AdamSPGD is more efficient than SPGD.

Optics EXPRESS

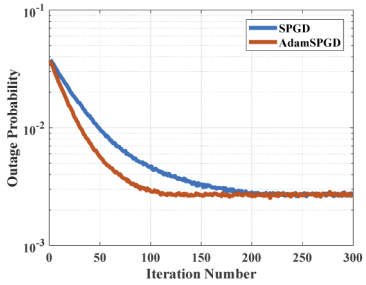

Fig. 7. Comparison of outage probability between SPGD and AdamSPGD.

The amplitude of random perturbation voltages in algorithms is worthy of discussion because of its significant impact on the performance. Thus, we evaluated the two algorithms under the same setting as the previous simulations, except for changing the value of Δu from 0.1 to 0.9, to further verify the robustness of AdamSPGD. The results are shown in **Fig. 8** that clearly show the high sensitivity of SPGD to Δu. When Δu is 0.1, the correction speed of SPGD is extremely low (**Fig. 8(a)**), and when Δu increases to 0.9, SPGD prematurely converges to the local optimum (**Fig. 8(c)**). In contrast, AdamSPGD still functions efficiently under $\Delta u \in [0.1, 0.9]$ (**Fig. 8(b), Fig. 8(d)**). The results show that AdamSPGD has a certain robustness over a wide range of Δu that is convenient for use in the practical applications of SLAO.

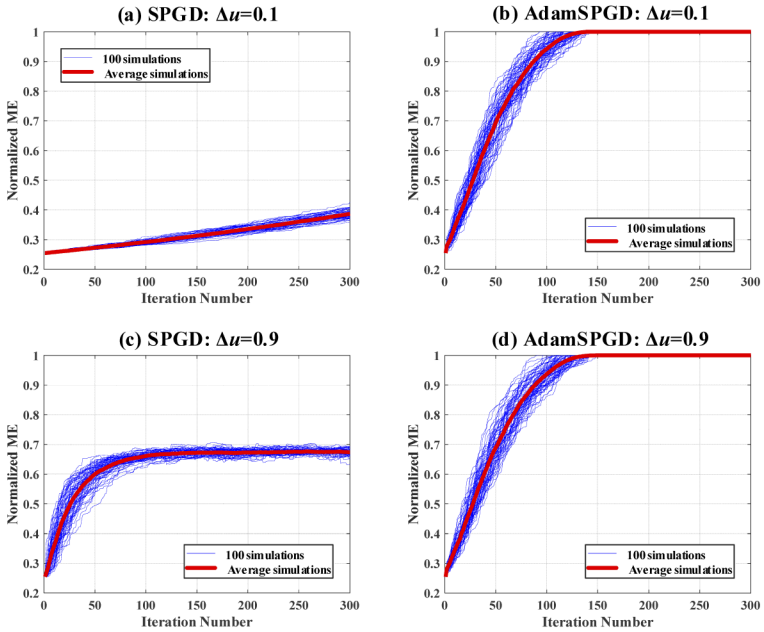

Fig. 8. Comparison of SPGD and AdamSPGD under different values of Δu.

Since researchers always use the parameter D/r0 to present the atmospheric turbulence strength, in this paper we directly change D/r0 to generate turbulence with different initial ME [10,37]. As D/r0 increases from 5 to 15, the initial ME of the wavefront generated by simulations becomes smaller, and we qualitatively define the turbulence intensity to be stronger. To further explore the correction performance of the two algorithms under different turbulence intensities, we also

Optics EXPRESS

demonstrate the relationship between ME and the iteration numbers under different turbulence conditions quantified as D/r0 in **Fig. 9**.

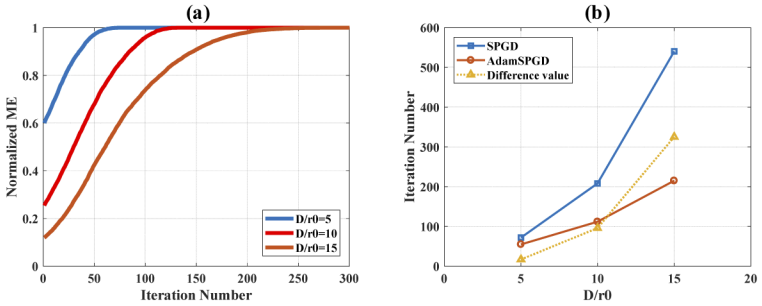

Fig. 9. Comparison of SPGD and AdamSPGD under different turbulence intensities. (a) Average correction curves using AdamSPGD, for D/r0 = 5, 10, and 15. (b) Number of iterations required for correction, and the difference between the two algorithms for different values of D/r0.

As shown in **Fig. 9(a)**, AdamSPGD can effectively correct the turbulence of different intensities, and as the intensity of turbulence increases, the correction speed gradually decreases. When D/r0 increases to 15, the correction speed is almost halved. **Figure 9(b)** illustrates that with the increase in turbulence intensity, the gap between the number of iterations required by the two algorithms increases. This shows that the stronger the turbulence intensity, the more obvious the advantages of AdamSPGD.

More efficient algorithms require fewer iterations, and faster CLCB can be achieved. Next, we verify the improvement of the algorithm in time-domain characteristics through simulations. First, we assume that the number of iterations is inversely proportional to CLCB, and the previous simulation results of AdamSPGD have achieved 100 Hz CLCB, considering the processing capacity of the FPGA and GPU-based high-performance processing platform. Thereafter, we can calculate the mean value of ME and BER at different Greenwood frequencies according to Eq. (3) and Eq. (4), and the results are shown in **Fig. 10**.

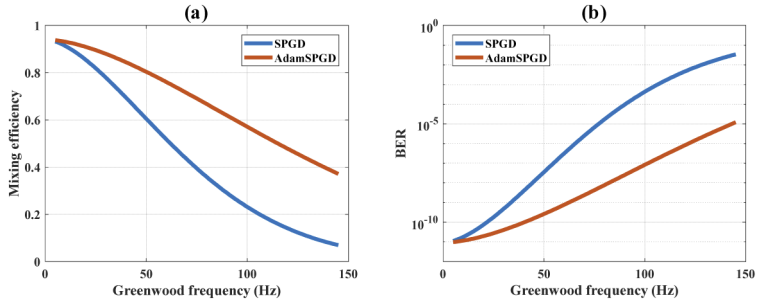

Fig. 10. Comparison of ME and BER between SPGD and AdamSPGD under different Greenwood frequencies. (a) The ME of the two algorithms varies with the Greenwood frequency. (b) The BER of the two algorithms varies with the Greenwood frequency.

Figure 10 illustrates that the dynamic ability of SLAO based on both algorithms degrades as the Greenwood frequency increases, and the attenuation in case of SPGD is more significant than that in case of AdamSPGD, implying that AdamSPGD exhibits improved dynamic performance and is more suitable for real-time systems compared with SPGD.

Optics EXPRESS

4.2. Experiment

To further investigate and verify the performance improvement of AdamSPGD in real-world application systems, we compare the two algorithms based on our SLAO experimental platform that is mainly composed of a laser, an HSC, and a 97-element CSDM. The structure and photograph of the platform are shown in **Fig. 11**.

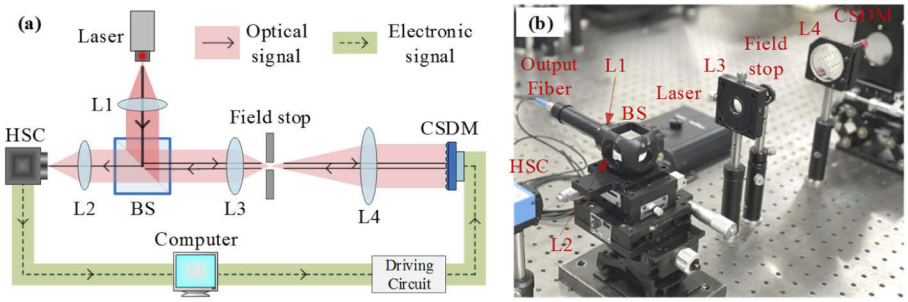

Fig. 11. (a) Structure of the SLAO experiment platform. The optical signal is colored in pink and the electronic signal is colored in green for convenient distinction. (b) Photograph of the SLAO experiment platform. L1–L4: lenses with focal length of 10 mm, 10 mm, 5 mm, and 15 mm, respectively.

As shown in **Fig. 11**, the SLAO experimental platform was constructed based on an auto-collimating optical system. The 635-nm laser beam is emitted from a single-mode optical fiber and collimated by lens L1, thereafter reflected by the BS and further expanded by L3 and L4 to match the size of the 97-element CSDM designed and manufactured by us. A field stop is added between lenses L3 and L4 to suppress stray light. After being reflected by the CSDM, the beam passes through L4, L3, and BS again, and is compressed and split. Finally, the beam reaches lens L2, and the speckle images are captured by the HSC. A computer is used to process the captured images, run the algorithms, and control the CSDM through the driving circuits to compensate for the aberrations.

In our experiments, we evaluated the performance of SPGD and AdamSPGD under the same initial conditions for a reasonable comparison. A set of CSDM initial control voltages are generated according to Zernike coefficients, and then the initial wavefront aberrations to be corrected are generated. The energy concentration rate of the speckle images captured by the HSC is used as the equivalent ME to reflect the performance of the SLAO. Although our experimental testbed is not a real communication system, nor is the ME here a real mixing efficiency, the flattening process of CSDM can simulate the correction process of atmospheric turbulence to verify the performance improvement of AdamSPGD compared to SPGD. According to simulation results, the optimal settings for SPGD are $\Delta u = 0.5$ and $\gamma = 2$, and the optimal settings for AdamSPGD are $\Delta u = 0.5$, $\alpha = 0.1$, $\beta_1 = 0.999$, $\beta_2 = 0.9$, and $\varepsilon = 10^{-8}$. An example of the experimental data is presented in Fig. 12.

From **Fig. 12**, we determine that the initial equivalent ME is ~0.0657 that significantly affects the system performance. The SPGD algorithm corrects gradually and converges at ~350 iterations. However, AdamSPGD dynamically adjusts the gain factor according to the gradient estimation for achieving rapid convergence. After ~186 iterations, the equivalent ME reaches 0.8828; therefore, AdamSPGD is 46.86% faster than SPGD.

Optics EXPRESS

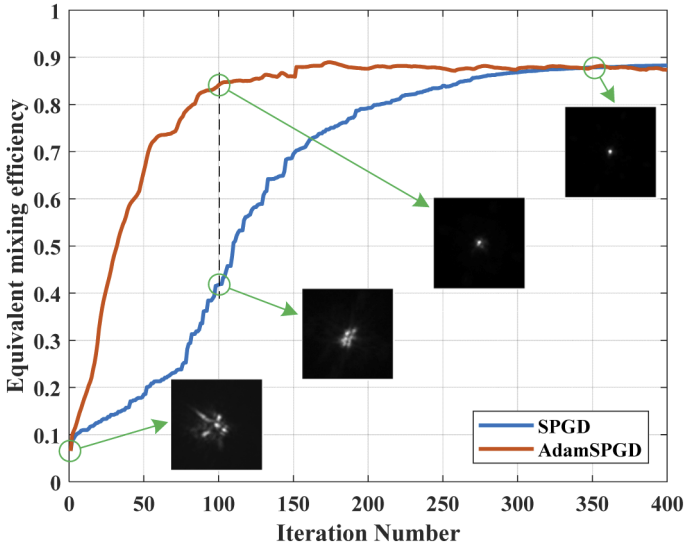

Fig. 12. Comparison of SPGD and AdamSPGD on the SLAO experiment platform.

5. Conclusion

In this paper, we propose an AdamSPGD algorithm that combines Adam and SPGD to compensate for wavefront aberrations more effectively. Detailed theoretical analysis and numerical simulations demonstrate that the negative influence of varying degrees of atmospheric turbulence on the ME, BER, and outage probability of the CFSOC system can be effectively suppressed by the designed algorithm. Specifically, owing to the addition of adaptive moment estimation to the conventional SPGD, AdamSPGD can not only accelerate the correction speed by ~50%, but also improve the robustness of parameters over a large range ($\Delta u \in [0.1, 0.9]$). Simultaneously, the stronger the turbulence intensity, more obvious are the advantages of AdamSPGD. In addition, as the Greenwood frequency increases, AdamSPGD exhibits improved dynamic capabilities, implying that the proposed algorithm is more suitable for real-time SLAO systems. In addition, experiments were conducted on both algorithms based on our proposed SLAO platform, and the results also indicate that AdamSPGD converges significantly faster. In conclusion, AdamSPGD is more effective for SLAO to improve communication quality and is a suitable alternative to SPGD. The findings of this study can provide guidance for the design of SLAO systems with excellent performance in CFSOC, and should be of interest to researches and engineers in the field of adaptive optics.

In the future, we intend to develop a high-performance processing platform based on FPGA and GPU, and apply the AdamSPGD to dynamic aberration correction experiments.

Funding. National Natural Science Foundation of China (62001448).

Disclosures. The authors declare no conflicts of interest.

Data availability. No data were generated or analyzed in the presented research.

References

1. M. Chen, C. Liu, D. Rui, and H. Xian, "Performance verification of adaptive optics for satellite-to-ground coherent optical communications at large zenith angle," Opt. Express **26**(4), 4230–4242 (2018).
2. C. Liu, M. Chen, S. Chen, and H. Xian, "Adaptive optics for the free-space coherent optical communications," Opt. Commun. **361**, 21–24 (2016).
3. M. Li and M. Cvijetic, "Coherent free space optics communications over the maritime atmosphere with use of adaptive optics for beam wavefront correction," Appl. Opt. **54**(6), 1453–1462 (2015).

Optics EXPRESS

4. J. Li, Z. Zhang, J. Gao, J. Sun, and W. Chen, "Bandwidth of adaptive optics system in atmospheric coherent laser communication," Opt. Commun. **359**, 254–260 (2016).
5. C. Liu, S. Chen, X. Li, and H. Xian, "Performance evaluation of adaptive optics for atmospheric coherent laser communications," Opt. Express **22**(13), 15554–15563 (2014).
6. A. Belmonte, "Influence of atmospheric phase compensation on optical heterodyne power measurements," Opt. Express **16**(9), 6756–6767 (2008).
7. J. Ma, K. Li, L. Tan, S. Yu, and Y. Cao, "Performance analysis of satellite-to-ground downlink coherent optical communications with spatial diversity over gamma-gamma atmospheric turbulence," Appl. Opt. **54**(25), 7575–7585 (2015).
8. L. Zuo, A. Dang, Y. Ren, and H. Guo, "Performance of phase compensated coherent free space optical communications through non-kolmogorov turbulence," Opt. Commun. **284**(6), 1491–1495 (2011).
9. J. Cao, X. Zhao, W. Liu, and H. Gu, "Performance analysis of a coherent free space optical communication system based on experiment," Opt. Express **25**(13), 15299–15312 (2017).
10. M. Chen, C. Liu, and H. Xian, "Experimental demonstration of single-mode fiber coupling over relatively strong turbulence with adaptive optics," Appl. Opt. **54**(29), 8722–8726 (2015).
11. J. Huang, H. Mei, K. Deng, L. Kang, W. Zhu, and Z. Yao, "Signal to noise ratio of free space homodyne coherent optical communication after adaptive optics compensation," Opt. Commun. **356**, 574–577 (2015).
12. H. Takenaka, M. Toyoshima, and Y. Takayama, "Experimental verification of fiber-coupling efficiency for satellite-to-ground atmospheric laser downlinks," Opt. Express **20**(14), 15301–15308 (2012).
13. M. Li, W. Gao, and M. Cvijetic, "Slant-path coherent free space optical communications over the maritime and terrestrial atmospheres with the use of adaptive optics for beam wavefront correction," Appl. Opt. **56**(2), 284–297 (2017).
14. L. Yang, K. Yao, J. Wang, J. Cao, X. Lin, X. Liu, W. Liu, and H. Gu, "Performance analysis of 349-element adaptive optics unit for a coherent free space optical communication system," Sci. Rep. **9**(1), 1–11 (2019).
15. S. Zhang, R. Wang, Y. Wang, H. Mao, G. Xu, Z. Cao, and L. Xuan, "Extending the detection and correction abilities of an adaptive optics system for free-space optical communication," Opt. Commun. **482**, 126571 (2021).
16. Z. Li, J. Cao, X. Zhao, and W. Liu, "Swarm intelligence for atmospheric compensation in free space optical communication—Modified shuffled frog leaping algorithm," Opt. Laser Technol. **66**, 89–97 (2015).
17. P. Yang, Y. Liu, M. Ao, S. Hu, and B. Xu, "A wavefront sensor-less adaptive optical system for a solid-state laser," Opt. Lasers Eng. **46**(7), 517–521 (2008).
18. H. Gu, M. Liu, H. Liu, X. Yang, and W. Liu, "An algorithm combining convolutional neural networks with SPGD for SLAO in FSOC," Opt. Commun. **475**, 126243 (2020).
19. Q. Yang, J. Zhao, M. Wang, and J. Jia, "Wavefront sensorless adaptive optics based on the trust region method," Opt. Lett. **40**(7), 1235–1237 (2015).
20. X. He, X. Zhao, S. Cui, and H. Gu, "A rapid hybrid wave front correction algorithm for sensor-less adaptive optics in free space optical communication," Opt. Commun. **429**, 127–137 (2018).
21. J. Cao, X. Zhao, Z. Li, W. Liu, and Y. Song, "Stochastic parallel gradient descent laser beam control algorithm for atmospheric compensation in free space optical communication," Optik **125**(20), 6142–6147 (2014).
22. Z. Huang, X. Tang, D. Zhang, X. Wang, Q. Hu, J. Li, and C. Liu, "Coherent beam combination of ten fiber arrays via stochastic parallel gradient descent algorithm," J. Opt. Technol. **82**(1), 16–20 (2015).
23. Y. Gong, K. Yang, H. Yong, J. Guan, G. Shentu, C. Liu, F. Li, Y. Cao, J. Yin, S. Liao, J. Ren, Q. Zhang, C. Peng, and J. Pan, "Free-space quantum key distribution in urban daylight with the SPGD algorithm control of a deformable mirror," Opt. Express **26**(15), 18897–18905 (2018).
24. H. Zhao, J. An, M. Yu, D. Lv, K. Kuang, and T. Zhang, "Nesterov-accelerated adaptive momentum estimation-based wavefront distortion correction algorithm," Appl. Opt. **60**(24), 7177–7185 (2021).
25. S. L. Lachinova and M. A. Vorontsov, "Performance analysis of an adaptive phase-locked tiled fiber array in atmospheric turbulence conditions," in *Proc. SPIE International Society for Optics and Photonics*, Vol. 5895 (2005).
26. K. Wu, Y. Sun, Y. Huai, S. Jia, X. Chen, and Y. Jin, "Multi-perturbation stochastic parallel gradient descent method for wavefront correction," Opt. Express **23**(3), 2933–2944 (2015).
27. Q. Hu, L. Zhen, Y. Mao, S. Zhu, X. Zhou, and G. Zhou, "Adaptive stochastic parallel gradient descent approach for efficient fiber coupling," Opt. Express **28**(9), 13141–13154 (2020).
28. G. Yang, L. Liu, Z. Jiang, T. Wang, and J. Guo, "Improved SPGD algorithm to avoid local extremum for incoherent beam combining," Opt. Commun. **382**, 547–555 (2017).
29. G. Yang, L. Liu, Z. Jiang, J. Guo, and T. Wang, "Incoherent beam combining based on the momentum SPGD algorithm," Opt. Laser Technol. **101**, 372–378 (2018).
30. J. Song, Y. Li, D. Che, J. Guo, and T. Wang, "Coherent beam combining based on the SPGD algorithm with a momentum term," Optik **202**, 163650 (2020).
31. D. Che, Y. Li, Y. Wu, J. Song, and T. Wang, "Theory of AdmSPGD algorithm in fiber laser coherent synthesis," Opt. Commun. **492**, 126953 (2021).
32. D. Kingma and J. Ba, "Adam: A method for stochastic optimization," arXiv preprint arXiv:1412.6980 (2014).
33. M. Niu, J. Cheng, and J. Holzman, "Exact error rate analysis of equal gain and selection diversity for coherent free-space optical systems on strong turbulence channels," Opt. Express **18**(13), 13915–13926 (2010).
34. R. J. Noll, "Zernike polynomials and atmospheric turbulence," J. Opt. Soc. Am. **66**(3), 207–211 (1976).

Optics EXPRESS

35. N. Roddier, "Atmospheric wavefront simulation using Zernike polynomials," Opt. Eng. **29**(10), 1174–1180 (1990).
36. S. Cui, X. Zhao, X. He, and H. Gu, "A Quick Hybrid Atmospheric-interference Compensation Method in a WFS-less Free-space Optical Communication System," Curr. Opt. Photonics **2**(6), 612–622 (2018).
37. H. Yang, X. Li, C. Gong, and W. Jiang, "Restoration of turbulence-degraded extended object using the stochastic parallel gradient descent algorithm: numerical simulation," Opt. Express **17**(5), 3052–3062 (2009).